JOURNAL OF MATERIALS SCIENCE 25 (1990) 4622–4629

# Continuous creep cavity nucleation by stochastic grain-boundary sliding

K. S. CHAN, R. A. PAGE
*Southwest Research Institute, San Antonio, Texas 78284, USA*

Creep cavitation in metals and ceramics is generally considered to occur by the nucleation, growth, and coalescence of grain-boundary cavities. By considering grain-boundary slidings as the process driving force, a stochastic model is proposed for continuous cavity nucleation in metals and ceramics subjected to creep loading. The nucleation rate is shown to be directly proportional to the number of grain-boundary sliding events. The dependence of the number of cavities on grain boundary sliding displacement, creep strain, and time are established and compared with available experimental data of alumina, copper, and copper alloys. This comparison supports the contention that creep cavity nucleation in metals and ceramics does originate from stochastic grain-boundary sliding.

## 1. Introduction

Cavity nucleation in metals and ceramics has generally been considered as a process which involves the condensation of vacancies on grain boundaries subjected to high local tensile stresses [1–3]. Theoretical analyses [2, 3] indicate that tensile stress required to form a spherical cavity is of the order of $E/100$, where $E$ is Young's modulus. Such a tensile stress is at least an order of magnitude higher than the service stresses at which cavities are observed in metals and ceramics. Thus, one or both of the following two things must be present in order for cavity nucleation to be feasible: (1) a local stress concentration of at least 10 to 20 at the potential cavity nucleation sites [3], and (2) the presence of favourable interfaces for the formation of non-spherical critical nuclei [1, 2, 4]. In some cases, a moderate stress concentration is required even for heterogeneous nucleation [4].

A variety of stress concentration sites and nucleation mechanisms, including stress concentration at particles, ledges, and triple points on sliding boundaries and the intersection of slip bands and grain-boundary particles, have been proposed for nucleating creep cavities in metals and ceramics (e.g., see [5–10]). By invoking stochastic grain-boundary sliding [3], most of the proposed mechanisms can generally provide the large local stress concentration required for nucleating cavities. The duration of the high tensile stress induced by sliding is, however, very short because of the competition of stress relaxation by diffusion [4]. In particular, Chan *et al.* [4] have shown that for a ledge on a sliding grain boundary, there exists only a small time period within which the local stress concentration is sufficiently large for cavity nucleation. Outside that time period, cavity nucleation is improbable because of an insufficient stress concentration. Thus, the relationship between stochastic grain-boundary sliding and continuous cavity nucleation remains unestablished. The objective of this paper is to quantify the role of the periodic, short-duration, grain-boundary sliding-induced stress "spikes" in the continuous nucleation of cavities in metals and ceramics. Stochastic grain-boundary sliding will be treated as a Poisson point process [11]. Accommodation of sliding grains by adjacent creeping grains will be considered. The cavity nucleation rate will be shown to depend on the number of stochastic grain-boundary sliding events. Expressions relating the number of cavities to grain-boundary sliding displacement, creep strain and time will be developed and compared with published data in the literature. The results of this work serve to demonstrate that stochastic grain-boundary sliding is the driving force for continuous cavity nucleation in metals and ceramics.

## 2. Stochastic grain-boundary sliding

It is envisioned that some of the grain boundaries in metals and ceramics subjected to creep loading would exhibit sliding in a stochastic manner, leading to stress concentrations and, therefore, cavity nucleation at inhomogeneities (particles, ledges, slip band intersections) located along the two-grain junctions or at triple-points. For clarity, the characteristics and current understanding of stochastic grain-boundary sliding is first reviewed.

Stochastic grain-boundary sliding has been experimentally observed in a number of materials [12], including copper [13], aluminium [14–17], tin [18], NaCl [19], and MgO [19] bicrystals. In the classic study of grain-boundary sliding in copper bicrystals, Intrater and Machlin [13] observed that each of the stochastic grain-boundary sliding events was distinct with the sliding distance/time curve, shown in Fig. 1, being characterized by null displacement periods and sudden displacement jumps. As pointed out recently by Page and Chan [20], those characteristics suggest


0022–2461/90 $03.00 + .12 

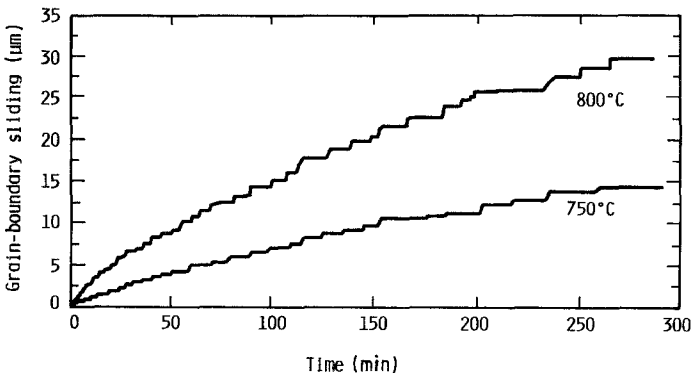


*Figure 1* Characteristics of stochastic grain-boundary sliding in copper bicrystal at 2.1 MPa from Intrater and Machlin [13].

that stochastic grain-boundary sliding satisfies the conditions for a point process [11]. In addition, the grain-boundary sliding process can also be considered to evolve without effects, i.e. the past sliding events have no influence on the future behaviour, when grain-boundary sliding occurs under constrained conditions, such as in a typical polycrystalline material. On the basis of these assumptions, the counting process of the sliding events can be represented as an ordinary continuous time stochastic process of the Poisson type. Thus, the number of sliding events with epochs in the time interval $(t_1, t_2)$ is described by the Poisson distribution, and the probability law of the stochastic sliding process is completely specified by its mean function, which represents the mean value of the number of grain-boundary sliding events.

A simple function, $\mu'(t)$, that satisfies the requirements for a Poisson process and can be used for describing the mean value of the number of grain-boundary sliding events at time $t$, is [20]

$$\mu'(t) = a_0 t^{1-m}/(1 - m) \quad (1)$$

where $a_0$ and $m$ are constants. To satisfy the conditions for a Poisson process, $a_0$ must be greater than zero ($a_0 > 0$) and $m$ must be less than unity ($m < 1$). Fig. 1 shows that the sliding displacement per event, though varying somewhat with time, can be considered as essentially constant for modelling purposes. If the average sliding distance for a sliding event is $\langle x \rangle$, the total grain-boundary sliding displacement, $U$, then becomes

$$U(t) = a_0 \langle x \rangle t^{1-m}/(1 - m) \quad (2)$$

leading to

$$\varepsilon_{gb}(t) = a_0 \langle x \rangle t^{1-m}/[l_0(1 - m)] \quad (3)$$

when the sliding displacement, $U$, is divided by the initial gauge length, $l_0$, of the specimen to obtain the average strain, $\varepsilon_{gb}$, due to grain-boundary sliding. The functional behaviour of Equations 2 and 3 is identical to typical creep curves, exhibiting transient, steady state, and tertiary regions when the value of $m$ is less than unity. Specifically, the value of $m$ ranges between zero and unity for transient behaviour, $m = 0$ for steady-state conditions, and $m < 0$ for tertiary sliding. The value of $m$ is expected to decrease with increasing time when sliding proceeds from the transient stage to the steady state and tertiary stages.

A review of the grain-boundary sliding measurements in the literature indicates that both Equations 2 and 3 provide good descriptions of the grain-boundary sliding displacement and strain for metals [21, 22], as illustrated in Fig. 2a for copper [22]. Thus, when modelled as a Poisson process, stochastic grain-boundary sliding leads to time-dependent displacement or strain curves that are reminiscent of the creep curves. Fig. 2b also shows that the ratio of $\varepsilon_{gb}/\varepsilon_t$, where $\varepsilon_t$ is the total macroscopic strain, in copper is relatively constant at 400° C and a stress of 17.9 MPa.

## 3. Accommodation of stochastic grain-boundary sliding

For compatibility reasons, stochastic grain-boundary sliding in polycrystalline materials must be accommodated by neighbouring grains. As a result, stochastic

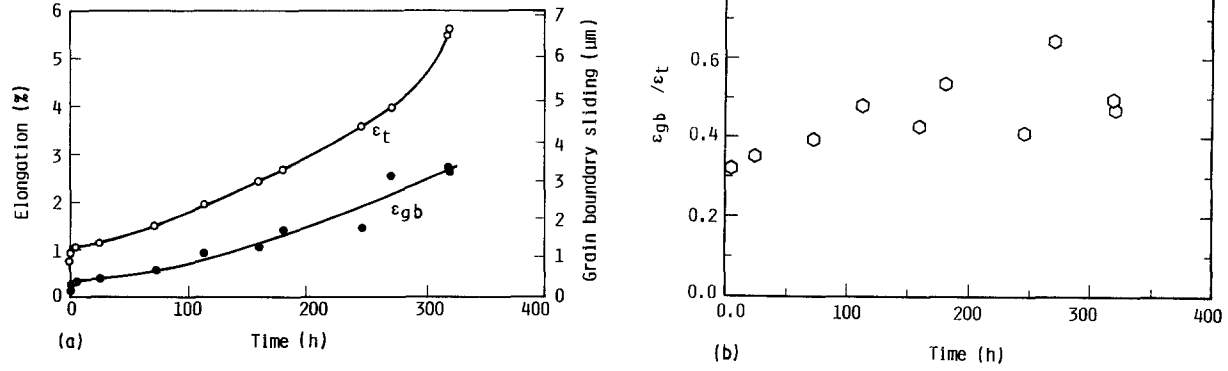


*Figure 2* Grain-boundary sliding displacement and creep curves of copper, at 400° C and 17.9 MPa, from McLean and Farmer [22]: (a) grain-boundary sliding displacement, grain-boundary sliding strain ($\varepsilon_{gb}$), and total creep strain ($\varepsilon_t$), and (b) $\varepsilon_{gb}/\varepsilon_t$ as a function of time.

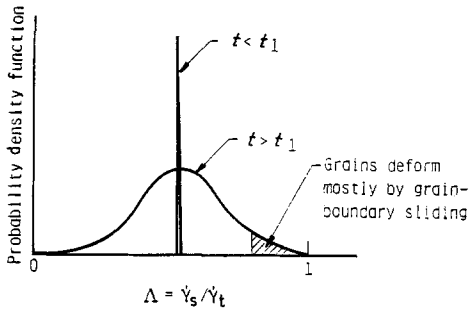


*Figure 3* A schematic drawing showing the changes in probability density function of grain sliding at a given value of $\Lambda$ with time as the result of stochastic grain-boundary sliding. Note that $\Lambda = 1$ for grains which deform by grain-boundary sliding only, and $\Lambda = 0$ for grains which deform by creep only. The majority of the grains deform by both creep and grain-boundary sliding.

grain-boundary sliding and, therefore, cavity nucleation can sometimes be controlled by diffusion and/or the deformation characteristics of the matrix, depending on the active accommodation process. Assuming full matrix accommodation, the contribution of stochastic grain-boundary sliding to the total, macroscopic strain rate, $\dot{\varepsilon}_t$, can be elucidated in a straightforward manner. If one considers a polycrystalline material containing grains that deform initially, at $t < t_1$, at a constant creep rate, $\dot{\varepsilon}_c$, and a constant sliding rate, $\dot{\varepsilon}_{gb}$, the total, macroscopic strain rate, $\dot{\varepsilon}_t$, then equals the sum of $\dot{\varepsilon}_c$ and $\dot{\varepsilon}_{gb}$ for fully accommodated sliding. Denoting $\dot{\varepsilon}_{gb}/\dot{\varepsilon}_t$ as $\Lambda$, the probability density function for the $i$th group of grains sliding at a given value of $\Lambda^i$ ($\Lambda^i = \dot{\varepsilon}^i_{gb}/\dot{\varepsilon}_t$) is then represented by the delta function, as illustrated in Fig. 3. At $t > t_1$, stochastic grain-boundary sliding is allowed to occur in some of the grains such that $V_i$ represents the volume fraction of the $i$th group of grains creeping at $\dot{\varepsilon}^i_c$ and sliding at $\dot{\varepsilon}^i_{gb}$. Under this condition,

$$\dot{\varepsilon}_t = \sum_{i=1}^{l} V_i(\dot{\varepsilon}^i_c + \dot{\varepsilon}^i_{gb}) = \dot{\varepsilon}_c + \dot{\varepsilon}_{gb} \quad (4)$$

with $l$ being the total number of groups of grains deforming and creeping at different values of $\Lambda^i$. For constrained deformation

$$\dot{\varepsilon}_t = \dot{\varepsilon}_{gb} + \dot{\varepsilon}_c \quad (5)$$

for all values of $\Lambda^i$ ranging from 0 to 1. Substituting Equation 5 into Equation 4 leads to $\Sigma V_i = 1$, as it should. For $t > t_1$, the probability density function for grains of a given $\Lambda^i$ is no longer described by the delta function, but instead by a function which shows a finite probability value for each possible value of $\Lambda^i$, as illustrated in Fig. 3. Thus, the volume fraction of grains sliding at a given value of $\Lambda^i$ can vary with time, even though the macroscopic strain rate, $\dot{\varepsilon}_t$, is constant for constrained deformation. Because grains which manifest large sliding components are the only likely sites for stress concentration, the number of eligible grain boundaries for cavity nucleation is limited by the shape of the distribution function near $\Lambda^i = 1$.

Experimental values of the ratio of grain-boundary sliding strain to total creep strain, $\Lambda$, have been reported for a large number of metals. From Equation 4

$$\Lambda = \frac{\varepsilon_{gb}}{\varepsilon_t} = \frac{\dot{\varepsilon}_{gb}}{\dot{\varepsilon}_t} = \sum_{i=1}^{l} V_i\Lambda^i \quad (6)$$

which indicates that the macroscopic grain-boundary sliding displacement measurements contain contributions of both the ratio of $\Lambda^i(\dot{\varepsilon}^i_{gb}/\dot{\varepsilon}^i_t)$ and the volume fraction, $V_i$, of individual grains undergoing stochastic grain-boundary sliding. The experimental results for copper [22] in Fig. 2 indicate that $\Lambda$ is relatively insensitive to time and is approximately constant for a particular temperature and stress; the probability of grain-boundary sliding is, therefore, essentially the same in the transient, steady-state, and tertiary creep regimes. Relatively constant values of $\Lambda$ which are independent of creep time but dependent on temperature and stress have also been observed in other metals, including aluminium, iron, zinc, and aluminium and copper alloys [22].

## 4. Stochastic grain-boundary sliding and cavity nucleation

Experimental evidence indicates that cavity nucleation in engineering alloys and metals generally requires both grain-boundary sliding and grain-boundary particles [1, 2, 23, 24] or ledges [4, 20, 25, 26]. In the former case, cavities have been found to nucleate preferentially at particles on sliding grain boundaries but not at sliding grain boundaries without particles [8, 27, 28]. In contrast, cavities in ceramics have been observed to nucleate near three-grain junctions (triple points) [29, 30], and then propagate along grain facets to form facet-sized cavities. Recent experimental evidence, based on transmission electron microscopy [4, 31] and small-angle neutron scattering measurements [32–36], has demonstrated that creep cavities in ceramics also nucleate at ledges along two-grain junctions. This observation has been noted in ceramics both with [31, 34–36] and without [4, 32, 33] grain-boundary amorphous phases. In all cases, stochastic grain-boundary sliding is required in order to achieve the stress concentration necessary for cavity nucleation

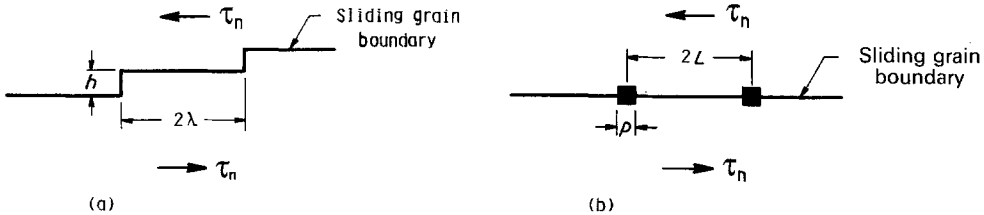


*Figure 4* Schematic drawings showing sliding of a grain boundary containing either (a) ledges or (b) particles.

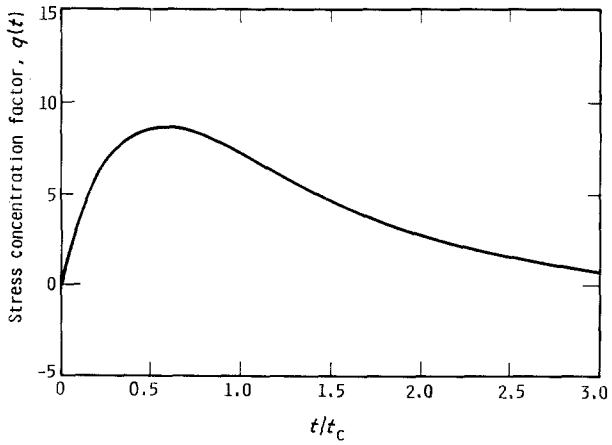


*Figure 5* Time-dependent stress concentration factor for a ledge on a sliding grain boundary, from Chan *et al.* [4]. Ledge height = 8 nm, ledge spacing = 400 nm; $\sigma(t) = q(t)\sigma_\infty = 2q(t)\tau_\infty$.

at grain-boundary particles [1, 2, 24, 37, 38], triple points [39] or ledges [4].

The time-dependent stress concentration factor, $q(t)$, for a ledge of height, $h$, and spacing, $\lambda$, on a sliding boundary is [4]

$$q(t) = \frac{\sigma(t)}{2\tau} = \frac{1}{2}\left\{\frac{\lambda}{h}[1 - \exp(-t/t_{BR})]\exp(-t/t_c) + c\right\} \quad (7)$$

with $c = \sigma_n/\tau_n$, where $\sigma_n$ and $\tau_n$ are the normal and shear stresses acting on the grain boundary prior to sliding (see Fig. 4a); $c = -1$ for compression and $c = 1$ for tension of a sliding boundary aligned at 45° to the stress axis. The characteristic time, $t_{BR}$, for grain-boundary relaxation is [3]

$$t_{BR} = \frac{1}{4}\left(\frac{kT}{GD_b\delta_b}\right)\left(\frac{\lambda}{b}\right)g(h/\lambda) \quad (8)$$

and it depends on the magnitude, $\boldsymbol{b}$, of the Burgers vector, temperature ($T$), ledge spacing, shear modulus ($G$), and the grain-boundary diffusivity ($D_b\delta_b$); $k$ is the Boltzmann constant and $g(h/\lambda)$ is the boundary-correction factor whose value depends on the ledge height to spacing ratio. The characteristic time, $t_c$, for relaxing the elastic stress concentration at the ledge by grain-boundary diffusion is [4]

$$t_c = \frac{(1 - \nu)kTh^3}{4\Omega D_b\delta_b G} \quad (9)$$

where $\nu$ is Poisson's ratio and $\Omega$ is the atomic volume. The time-dependent stress concentration factor for a particle size, $p$, and spacing, $L$, on a sliding boundary (Fig. 4b) can be obtained using the same approach employed in the ledge model of Chan *et al.* [4]. The analysis indicates that replacing $\lambda$ with $L$ and $h$ with $p$ in Equations 7, 8, and 9 lead to the appropriate equations for the time-dependent stress concentration factor for a particle on a sliding boundary.

TABLE I Material constants for sintered $Al_2O_3$ (Lucalox) at 1600° C

| Constants | Values |
|---|---|
| $\Omega$ | $4.2 \times 10^{-29}$ m$^3$ |
| $D_b\delta_b$ | $2.7 \times 10^{-21}$ m$^3$ sec$^{-1}$ |
| $G$ | $1.182 \times 10^5$ MPa |
| $\boldsymbol{b}$ | $4.76 \times 10^{-10}$ m |
| $k$ | $1.38 \times 10^{-23}$ J K$^{-1}$ |
| $\gamma_s$ | 1 J M$^{-2}$ |
| $n_0$ | $1 \times 10^{18}$ m$^{-3}$ |

The time-dependent behaviour of the stress concentration at a ledge on a 45° sliding boundary is illustrated in Fig. 5 for a Lucalox alumina subject to a compressive stress of 140 MPa at 1600° C. The relevant material properties required for this calculation are summarized in Table I; the ledge height is 8 nm, and the ledge spacing is 400 nm. The stress concentration factor, $q(t)$, is seen to first increase but then decreases with time, resulting in a maximum stress concentration factor of 8.5 at $t/t_c = 0.6$. The time period over which a high stress concentration factor (e.g. $q(t) > 5$) exists, however, only lasts about one characteristic $t_c$, which is 165 nsec for this particular case. It is only within this extremely short time period that cavities can nucleate and grow beyond a critical size.

If one considers thermal nucleation, the rate of cavity nucleation, $\dot{n}$, is given by [1, 24, 39]

$$\dot{n} = \dot{N}n_0 \quad (10)$$

with

$$\dot{N} = 4\pi\gamma_s Z \sin\alpha/[\sigma(t)\Omega^{4/3}]D_b\delta_b \times \exp[-4\gamma_s^3 F_v/(\sigma(t)^2 kT)] \quad (11)$$

where $n_0$ is the number of available nucleation sites per unit volume, $Z$ is the Zeldovich non-equilibrium factor, $\gamma_s$ is the surface energy of the cavities, $\sigma(t)$ is the normal stress across the grain boundary, and $F_v$ is the cavity shape parameter which yields the volume of the critical nucleus when multiplied by $R^3$ with $R$ being the critical radius. The cavity nucleation rate is generally dominated by the exponential term in Equation 11 which gives a threshold-like behaviour. The importance of the large transient local tensile stress induced at grain-boundary ledges or particles by stochastic grain-boundary sliding is, therefore, quite obvious.

Using material properties listed in Table I, the nucleation kinetics of creep cavities at a ledged grain

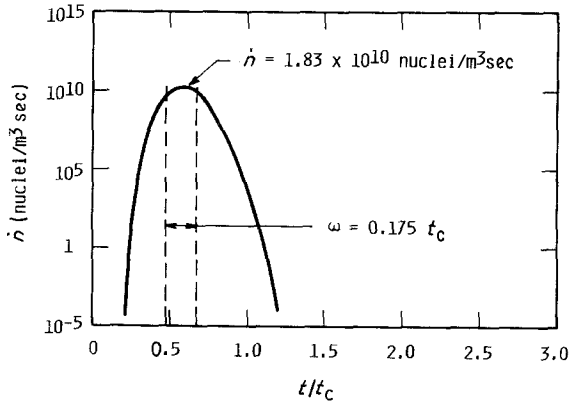


*Figure 6* Cavity nucleation rate as a function of time normalized by the characteristic time, $t_c$. Note that most of the cavities are nucleated near the peak of the transient stress pulse whose effective width is $\omega$.

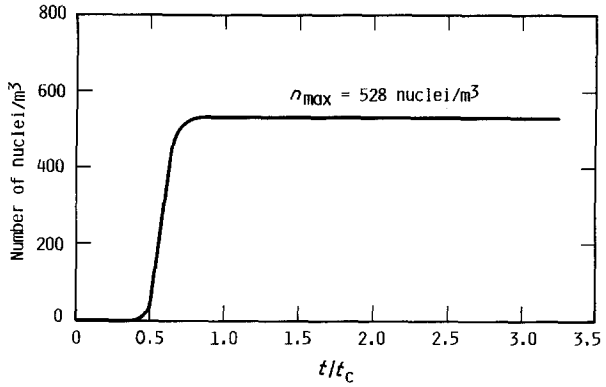


*Figure 7* Number of cavities as a function of time normalized by the characteristic time, $t_c$. The total number of cavities nucleated is 528 nuclei/m$^3$ which remains unchanged with increasing time for $t \geqslant 0.8t_c$. No cavities are nucleated until $t > 0.45t_c$.

boundary in Lucalox alumina has been calculated by combining Equations 7, 10, and 11 and integrating numerically with time. The nucleation rate and number of cavity nuclei corresponding to the time-dependent stress concentration factor in Fig. 5 are presented in Figs 6 and 7, respectively. As expected, the maximum nucleation rate is observed at the maximum value of $q(t)$. The number of cavities nucleated is 528 m$^{-3}$. The period, $\omega$, during which cavity nucleation can occur is only 30 nsec, which is approximately $0.175t_c$. Furthermore, almost all of the cavities are formed at or near the peak of the transient stress pulse. Outside this period, the stress concentration is insufficient to cause cavity nucleation. Thus, $\omega$ can be considered as the effective width of the transient stress pulse during which all the cavities are nucleated.

Nucleation kinetics calculations have also been performed as a function of the ledge height to spacing ratio. The maximum value of the transient stress concentration factor, $q(t)$, has been found to depend on the ratio of $h/\lambda$, as shown in Fig. 8. Specifically, a low stress concentration factor occurs at a small ledge height because grain-boundary diffusion is effective in relaxing the local tensile stress induced by grain-boundary sliding, primarily due to a short diffusion distance. As the ledge height is increased, the diffusion distance and the ledge area supporting the local tensile stress are both increased. Because these two factors produce opposite effects on stress concentration, the value of $q(t)$ exhibits a maximum in a manner shown in Fig. 8. The consequence is that there exists a small

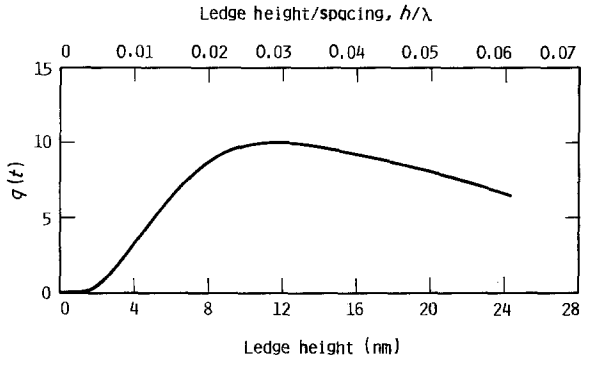


*Figure 8* Time-dependent stress concentration factor, $q(t)$, as a function of ledge height at a constant ledge space of 400 nm.

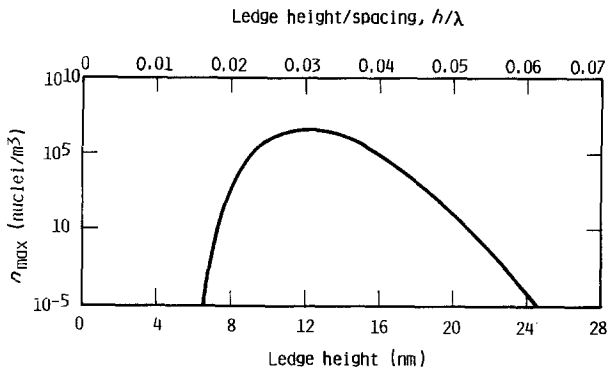


*Figure 9* The total number of cavities nucleated, $n_{max}$, as a function of ledge height at $\lambda = 400$ nm.

range of $h/\lambda$ ratios within which most of the cavity nuclei are produced, as depicted in Figs 9 and 10 which show $\dot{n}$ and the number of nuclei formed for various $h/\lambda$ values. The effective width, $\omega$, of the stress pulse is shown in Fig. 11 in terms of both the characteristic time, $t_c$, and the actual time period in which cavity nucleation occurs. The range of $h/\lambda$ within which cavities are formed is 0.015 to 0.055. Outside this range $\dot{N} \approx 0$ and the number of cavities formed is negligible (less than 1 nucleus/m$^3$). Thus, the presence of ledges on a sliding boundary is not a sufficient condition for cavity nucleation to occur; a proper or eligible ledge height to spacing ratio is also required. Similarly, a particle size to spacing of 0.015 to 0.055 is also necessary for cavity nucleation at particles on sliding grain boundaries.

Based on these results, it becomes apparent that grain-boundary sliding can be a source of continuous cavity nucleation only if the process occurs repeated over an extended period of time, i.e. the number of sliding events must increase with time. In other words, continuous cavity nucleation requires stochastic grain-boundary sliding of the Poisson type. Additionally, eligible nucleation sites must also be present on the grain boundaries. For these two reasons, it is more appropriate to write the cavity nucleation rate as

$$\dot{n} = \dot{N}(h/\lambda)\Gamma_0(h/\lambda)/D \qquad (12)$$

where $D$ is the grain size, $\Gamma_0$ is the number of eligible

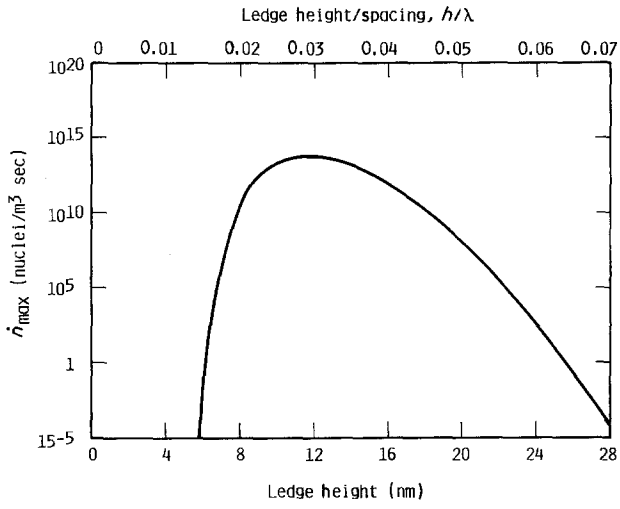


*Figure 10* The maximum nucleation rate, $\dot{n}_{max}$, as a function of ledge height at $\lambda = 400$ nm.

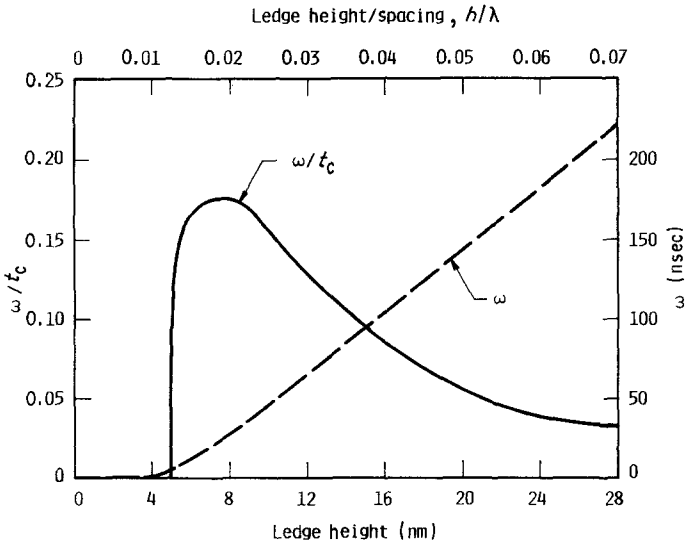


*Figure 11* The effective width (time period), $\omega$, of the transient stress pulse within which cavities are nucleated as a function of ledge height at $\lambda = 400\,\text{nm}$.

nucleation sites per unit area of an individual sliding grain boundary, and $\dot{N}$ is given by Equation 11. Both $\Gamma_0$ and $\dot{N}$ are functions of $h/\lambda$. Because all of the cavities are nucleated near the peak of the transient stress pulse ($\dot{N} = 0$ outside $\omega$), the number of cavities, $N_c/V$ is thus given by

$$\frac{N_c}{V} = \int_0^\infty \dot{n}\,dt$$

$$= \dot{N}_{max}(h/\lambda)\omega(h/\lambda)\Gamma_0(h/\lambda)/D \quad (13)$$

where $\dot{N}_{max}$ is the maximum nucleation rate evaluated at the minimum value of $q(t)$. When all of the stochastic grain-boundary sliding events are considered

$$\frac{N_c}{V} = \sum_{h/\lambda=0}^{h/\lambda=\infty} \mu_1(t)\dot{N}_{max}(h/\lambda)\omega(h/\lambda)\Gamma_0(h/\lambda)/D \quad (14)$$

leading to

$$\frac{N_c}{V} = \mu'(t)F \quad (15)$$

with

$$F = \frac{1}{D}\sum_{h/\lambda=0.015}^{h/\lambda=0.055} \dot{N}_{max}(h/\lambda)\omega(h/\lambda)\Gamma_0(h/\lambda) \quad (16)$$

because $\dot{N}_{max}(h/\lambda)\omega(h/\lambda) = 0$ for values of $h/\lambda$ lying outside the eligible range ($0.015 < h/\lambda > 0.055$).

An important feature of Equation 15 is that it relates the number of cavities directly to the mean function, $\mu'(t)$, representing the number of stochastic grain-boundary sliding events. Because the grain-boundary sliding displacement is also directly related to $\mu'(t)$, the relation between $N_c/V$ and grain-boundary displacement can be established by combining Equations 2 and 15, yielding

$$\frac{N_c}{V} = \frac{FU(t)}{\langle x\rangle} \quad (17)$$

leading to

$$\frac{N_c}{V} = \frac{Fl_0}{\langle x\rangle}\varepsilon_{gb}(t) \quad (18)$$

and

$$\frac{N_c}{V} = \frac{Fl_0\Lambda}{\langle x\rangle}\varepsilon_t(t) \quad (19)$$

when Equations 3 and 6 are substituted into Equation 17, respectively.

One of the significant findings of the proposed model is an expression relating cavity density to the number of stochastic grain-boundary sliding events, which appears to be the first of its kind. Combining

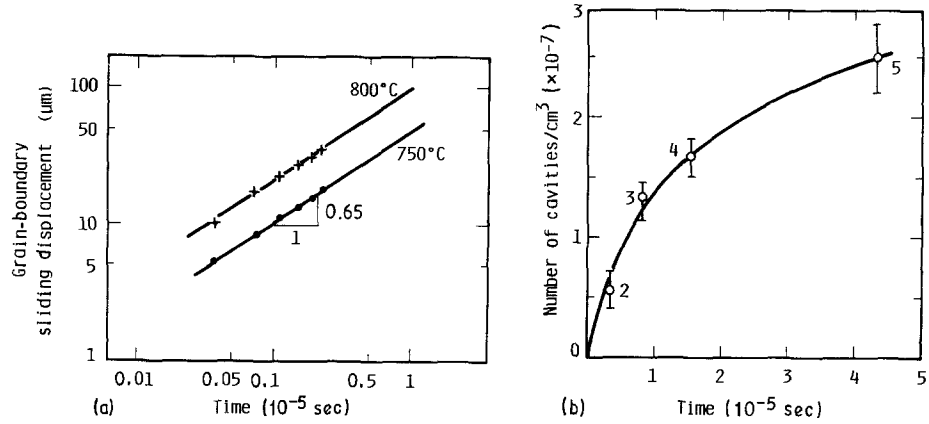


*Figure 12* The time dependence of grain-boundary sliding and number of cavities in copper: (a) grain-boundary sliding displacement plotted against time, from Intrater and Machlin [13], applied stress = 2.1 MPa, $u \propto t^{0.65}$, and (b) number of cavities per volume, $N_c/V$, plotted against time for copper at 400°C, 40 MPa, from Gittens [40], $N_c/V \propto t^{0.5}$. The proposed cavity nucleation theory predicts the same time exponent for both grain-boundary sliding and $N_c/V$.

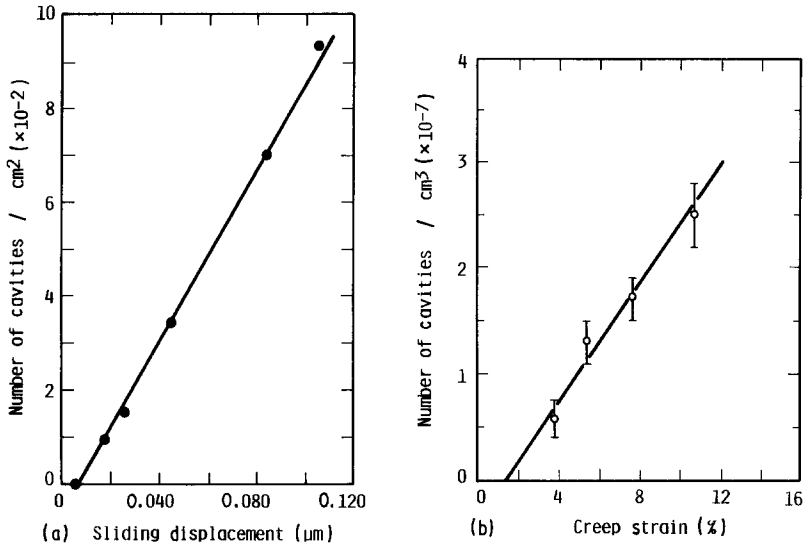


*Figure 13* Linear dependence of number of cavities per volume, $N_c/V$, or per area, $N_c/A$, on grain-boundary sliding displacement and creep strain: (a) $N_c/A$ against grain-boundary sliding displacement for a copper alloy at 11 MPa, 923 K, from Fleck *et al.* [41], and (b) $N_c$/V against creep strain for copper at 400° C, 40 MPa, from Greenwood [42]. (a) $N_c/A \propto N_c/V \propto u$, (b) $N_c/V \propto \varepsilon_t$.

Equations 1 and 15 leads to

$$\frac{N_c}{V} = \frac{a_0 F}{1 - m} t^{1-m} \tag{20}$$

and the conclusion that the cavity nucleation and stochastic grain-boundary sliding rates must have the same time exponent, primarily because of their dependence on the number of sliding events. The consequences of an identical time exponent in the cavity nucleation and sliding kinetics are linear relationships between cavity density, grain-boundary sliding displacement and strain, and creep strain.

Experimental evidence verifying the proposed relationships between the cavity density and creep time, grain-boundary sliding displacement and strain, and creep strain are shown in Figs 12 to 15. In Fig. 12a, the time exponent for the grain-boundary sliding displacement in copper is shown to be 0.65 [13]. According to the proposed theory, the time exponent, $\beta$ ($\beta = 1 - m$), for the cavity density should also be 0.65, being identical to that for grain-boundary sliding. As shown in Fig. 12b, the observed value is 0.5 [40]. For most metals, $\beta$ ranges from 0.38 to 1.0 [20]. The predicted linear relationship between $N_c/V$ and grain-boundary sliding displacement has been observed in a copper alloy [41] as shown in Fig. 13a, and the linear relation between $N_c/V$ and creep strain has been demonstrated for copper [42], as shown in Fig. 13b. Previously, Dyson [43] has also shown a linear behaviour between $N_c/V$ and creep strain for iron, steels, and a nickel-based alloy (Nimonic 80A). The results in Figs 12 and 13 demonstrate the intimate relationship between stochastic grain-boundary sliding and cavity nucleation in metals. In particular, these results demonstrate that stochastic grain-boundary sliding is present throughout the creep process, including the transient, steady-state, and tertiary regions. It contributes to the macroscopic creep strain as well as providing the local tensile stresses for cavity nucleation throughout the three stages of creep.

For the ceramic systems for which nucleation data have been obtained, values of $\beta$ ranging from 0.19 to 1.0 have been observed [20]. These results are quite similar to the $\beta$ values ranging from 0.38 to 1.0 that have been obtained for metallic materials. Unfor-

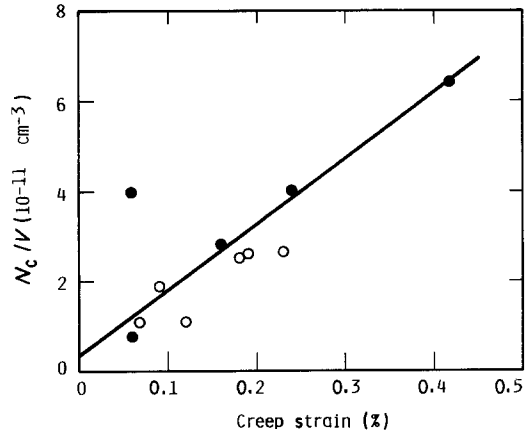


*Figure 14* Linear dependence of number of cavities on creep strain observed in AD99 alumina at 1300° C. Plot is based on data of Page *et al.* [36]. $\sigma$ = (●) 26 MPa, (○) 48 MPa.

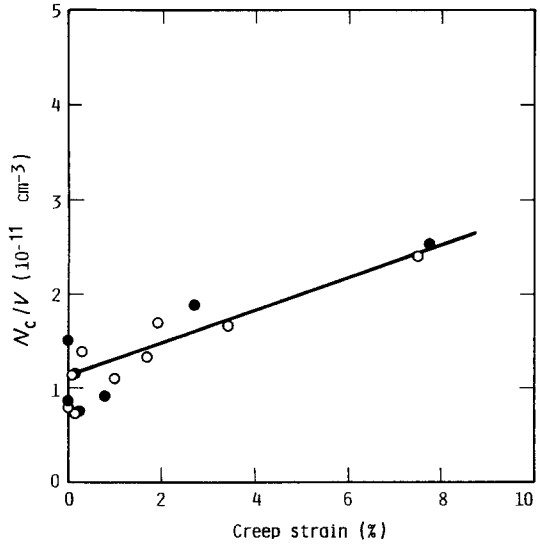


*Figure 15* Linear dependence of number of cavities on creep strain observed in Lucalox alumina at 1600° C. Plot is based on data of Page *et al.* [45]. Grain size = (●) 20 μm, (○) 37 μm.

tunately, grain-boundary sliding displacement data, however, are not presently available for any of the ceramic systems. It is, therefore, not possible to make a direct comparison between theory and experiment for the ceramic systems at the present time. Despite this fact, experimental evidence suggests that cavity nucleation in ceramics also originates from stochastic grain-boundary sliding; both grain-boundary ledges of height ranging from $\approx 4$ [44] to 20 nm [36] and cavities nucleated at grain-boundary ledges (see [4]) have been reported. Additionally, a linear relationship between $N_c/V$ and creep strain have been observed in AD99 alumina and in Lucalox alumina, as shown in Figs 14 and 15, respectively. Thus, it appears that stochastic grain-boundary sliding is the most likely driving force for continuous cavity nucleation in both metals and ceramics.

## 5. Conclusions

1. Stochastic grain-boundary sliding has been identified as the most likely driving force for continuous cavity nucleation in both metals and ceramics.

2. The number of cavities nucleated in metals and ceramics under creep loading is directly related to the number of stochastic grain-boundary sliding events. The cavity nucleation and grain-boundary sliding rates are predicted to have the same time exponent.

3. The dependence of the cavity density on grain-boundary sliding displacement, strain, and creep time are correctly predicted when stochastic grain-boundary sliding is modelled as a Poisson point process.

4. Cavity nucleation induced by stochastic grain-boundary sliding occurs within a small time period after the commencement of sliding and within a small range of ledge height to spacing or particle size to spacing ratios only.


## Acknowledgements

This work was supported by the U.S. Department of Energy, Office of Basic Energy Science, through Grant no. DE-FG05-84ER45063.


## References


1. R. RAJ and M. F. ASHBY, *Acta Metall.* **23** (1975) 653.
2. R. RAJ, *ibid.* **26** (1978) 995.
3. A. S. ARGON, I. W. CHEN and C. W. LAU, in "Creep-Fatigue-Environment Interactions", edited by R. M. Pelloux and N. S. Stoloff (Metallic Society AIME, New York, 1980) pp. 46–85.
4. K. S. CHAN, R. A. PAGE and J. LANKFORD, *Acta Metall.* **34** (1986) 2361.
5. A. J. PERRY, *J. Mater. Sci.* **9** (1974) 1016.
6. M. H. YOO and H. TRINKAUS, *Metall. Trans.* **14A** (1983) 547.
7. W. D. NIX, *Scripta Metall.* **17** (1983) 1.
8. A. S. ARGON, *ibid.* **17** (1983) 5.
9. S. H. GOODS and T. G. NIEH, *ibid.* **17** (1983) 17.
10. B. F. DYSON, *ibid.* **17** (1983) 31.
11. H. J. LARSON and B. O. SHUBERT, in "Probabilistic Models in Engineering Sciences", Vol. 2 (Wiley, New York, 1979) pp. 544–83.
12. H. GLEITER and B. CHALMER, *Prog. Mater. Sci.* **16** (1972) 179.
13. J. INTRATER and E. MACHLIN, *J. Inst. Metals* **88** (1959–60) 305.
14. F. N. RHINES, W. E. BOND and M. A. KISSEL, *Trans. ASM* **48** (1956) 919.
15. S. K. TUNG and R. MADDIN, *Trans. AIME* **209** (1957) 905.
16. F. WEINBERG, *Acta Metall.* **2** (1954) 889.
17. F. WEINBERG, *Trans. AIME* **212** (1985) 808.
18. K. E. PUTLICK and R. KING, *J. Inst. Metals* **80** (1951–52) 537.
19. M. A. ADAMS and G. T. MURRAY, *J. Appl. Phys.* **33** (1962) 2126.
20. R. A. PAGE and K. S. CHAN, *Metall. Trans.* **18A** (1987) 1843.
21. D. McLEAN and M. H. FARMER, *J. Inst. Metals* **83** (1954) 1.
22. *Idem, ibid.* **85** (1956) 41.
23. A. J. PERRY, *J. Mater. Sci.* **9** (1974) 1016.
24. J. S. WANG, J. J. STEPHENS and W. D. NIX, *Acta Metall.* **33** (1985) 109.
25. R. D. GIFKINS, *ibid.* **4** (1956) 98.
26. T. WATANABE, *Metall. Trans.* **14A** (1983) 531.
27. I. SERVI and N. J. GRANT, *Trans. AIME* **191** (1951) 909.
28. N. J. GRANT and A. W. MULLENDORE, "Deformation and Fracture at Elevated Temperatures" (Massachusetts Institute of Technology, Cambridge, 1965).
29. A. G. EVANS and A. S. RANA, *Acta Metall.* **28** (1980) 129.
30. H. HUBNER and J. STARK, "High Tech Ceramics" Part B, edited by P. Vencenzini (Elsevier, Amsterdam, 1987) p. 1247.
31. S. M. WIEDERHORN, B. J. HOCKEY, R. F. KRAUSE Jr and K. JAKUS, *J. Mater. Sci.* **21** (1986) 810.
32. R. A. PAGE and J. LANKFORD, *J. Amer. Ceram. Soc.* **66** (1983) C-146.
33. R. A. PAGE, J. LANKFORD and S. SPOONER, *Acta Metall.* **32** (1984) 3360.
34. *Idem, ibid.* **32** (1984) 1275.
35. J. LANKFORD, K. S. CHAN and R. A. PAGE, in "Fracture Mechanics of Ceramics", edited by R. C. Bradt, A. G. Evans, D. P. H. Hasselman and F. F. Lange (Plenum Press, New York, 1986) p. 327.
36. R. A. PAGE, J. LANKFORD, K. S. CHAN, K. HARDMAN-PHYNE and S. SPOONER, *J. Amer. Ceram. Soc.* **70** (1987) 137.
37. I. W. CHEN and A. S. ARGON, in "Creep and Fracture of Engineering Materials and Structures", edited by B. Wilshire and D. R. J. Owen (Pineridge Press, Swansea, UK, 1981) p. 289.
38. A. S. ARGON, in "Recent Advance in Creep and Fracture of Engineering Materials and Structures", edited by B. Wilshire and D. R. J. Owen (Pineridge Press, Swansea, UK, 1982) pp. 1–52.
39. A. G. EVANS, J. R. RICE and J. P. HIRTH, *J. Amer. Ceram. Soc.* **63** (1980) 368.
40. A. GITTENS, *Met. Sci. J.* **1** (1967) 214.
41. R. G. FLECK, D. M. R. TAPLIN and C. J. BEEVERS, *Acta Metall.* **23** (1975) 415.
42. G. W. GREENWOOD, *Phil. Mag.* **19** (1969) 423.
43. B. F. DYSON, *Scripta Metall.* **17** (1983) 31.
44. K. J. MORRISSEY and C. B. CARTER, *J. Amer. Ceram. Soc.* **67** (1984) 292.
45. R. A. PAGE, J. LANKFORD and S. SPOONER, *J. Mater. Sci.* **19** (1984) 3360.



*Received 19 July*
*and accepted 22 November 1989*